Engineering of Hollow Core–Shell Interlinked Carbon Spheres for Highly Stable Lithium–Sulfur Batteries

Qiang Sun, Bin He, Xiang-Qian Zhang, and An-Hui Lu*

State Key Laboratory of Fine Chemicals, School of Chemical Engineering, Dalian University of Technology, Dalian 116024, P.R. China

ABSTRACT We report engineered hollow core–shell interlinked carbon spheres that consist of a mesoporous shell, a hollow void, and an anchored carbon core and are expected to be ideal sulfur hosts for overcoming the shortage of Li–S batteries. The hollow core–shell interlinked carbon spheres were obtained through solution synthesis of polymer spheres followed by a pyrolysis process that occurred in the hermetical silica shell. During the pyrolysis, the polymer sphere was transformed into the carbon core and the carbonaceous volatiles were self-deposited on the silica shell due to the blocking effect of the hermetical silica shell. The gravitational force and the natural driving force of lowering the surface energy tend to interlink the carbon core and carbon/silica shell, resulting in a core–shell interlinked structure. After the SiO_2 shell was etched, the mesoporous carbon shell was generated. When used as the sulfur host for Li–S batteries, such a hierarchical structure provides access to Li^+ ingress/egress for reactivity with the sulfur and, meanwhile, can overcome the limitations of low sulfur loading and a severe shuttle effect in solid carbon-supported sulfur cathodes. Transmission electron microscopy and scanning transmission electron microscopy images provide visible evidence that sulfur is well-encapsulated in the hollow void. Importantly, such anchored-core carbon nanostructures can simultaneously serve as a physical buffer and an electronically connecting matrix, which helps to realize the full potential of the active materials. Based on the many merits, carbon–sulfur cathodes show a high utilization of sulfur with a sulfur loading of 70 wt % and exhibit excellent cycling stability (*i.e.*, 960 mA h g^{-1} after 200 cycles at a current density of 0.5 C).

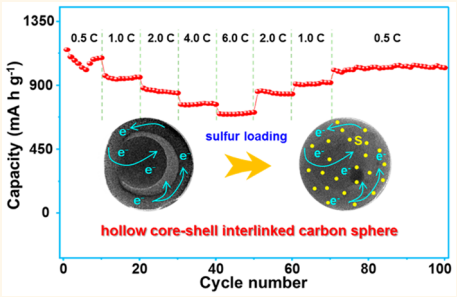

KEYWORDS: core–shell · Li–S battery · porous carbon · hollow structure · self-deposition

The lithium–sulfur (Li–S) battery is believed to be a very prominent candidate for next-generation high-energy density rechargeable power systems due to its high theoretical capacity, natural abundance, and low cost of sulfur.[1−4] The high capacity is based on the conversion reaction of sulfur to form lithium sulfide by reversibly incorporating two electrons per sulfur atom, whereas only one or less than one electron per transition metal ion can be utilized in the insertion-oxide cathodes. However, the high resistance of sulfur and lithium sulfide, the inevitable shuttle effect, and the self-discharge resulting from the dissolution of polysulfide intermediates along with the structure changes give rise to low sulfur utilization, poor cycle life of the sulfur cathode, and low Coulombic efficiency.[5−12]

To address these issues, most efforts focused on developing smart conductive porous materials and then immobilizing sulfur to keep sulfur particles electrically connected and limit polysulfide dissolution.[1,3,13] Exciting progress has recently been made in trapping active material in electrically conductive porous carbon since this concept was first presented by Wang *et al.*[6,14−19] A pioneering work was carried out by Nazar's group, in which ordered mesoporous carbon was first used for sulfur encapsulation and an initial specific capacity of *ca.* 1320 mA h g^{-1} can be reached.[20] After that, various carbonaceous materials including carbon sheets, hollow spheres, carbon nanotubes/fibers, graphene, and some composites of the above structures have been widely investigated as quick cures for the problems described above.[21,22]

Hollow carbon spheres with a large interior void and porous shell are eagerly expected for the immobilization of the high amount of starting active sulfur and polysulfides to

* Address correspondence to anhuilu@dlut.edu.cn.

Received for review June 9, 2015 and accepted July 16, 2015.

Published online July 16, 2015
10.1021/acsnano.5b03488

suppress their dissolution into the liquid electrolyte.[23−27] However, most studies show that sulfur was preferentially accommodated in the porous shell rather than in the interior space.[14,26−28] The main reason lies in the absence of strong adsorption potential in the interior, and thus no great driving force could suck the active sulfur particles passing through the porous shell and simultaneously settle down the polysulfide intermediates. So, an important concern is how to tactically engineer the structure of hollow carbon nanospheres that allows for maximum loading of sulfur in the hollow space and inhibition of polysulfide dissolution while keeping good electrolyte and lithium ion transport into the interior space.

In general, the micropore, presenting strong adsorption potential, has been demonstrated as the ideal container for accommodating and immobilizing the active material.[6,29−31] Based on the fact that the S−S bond length is in the range of 0.189−2.066 nm in sulfur allotropes,[32] the mesopore with a pore size smaller than 3 nm can also work with the micropore to imbibe sulfur and trap the disolved polysulfides by capillary forces and can improve lithium ion and electrolyte access.[20,33−37] However, large mesopores and macropores will not function in the trap polysulfide dissolution due to their open structures.[24,27,38] Hence, it is supposed that a feasible way of getting the utmost out of the present interior void of a hollow carbon sphere is to properly place microporous media in the hollow interior and create smaller mesopores in the shell.

Inspired by this idea, we designed hollow core−shell interlinked carbon spheres through a solution synthesis of the polymer followed by pyrolysis and self-deposition in a hermetical silica shell. Different from the traditional hollow spheres or core−shell structures, such hollow core−shell interlinked carbon spheres consist of a mesoporous carbon shell, a hollow void, and a microporous carbon core locally anchored to the shell, which are expected to be an ideal sulfur host to overcome the shortage of Li−S batteries. With the desired result, the carbon−sulfur cathodes show a high loading and utilization of sulfur and exhibit excellent cycling stability (*i.e.*, 960 mA h g^{-1} after 200 cycles at a current density of 0.5 C).

RESULTS AND DISCUSSION

Several methods have been proposed to engineer hollow carbon spheres with or without a core, but core−shell interlinked carbon spheres with hollow voids have never been developed. Such structures were denoted as hollow core−shell interlinked carbon spheres in this study and are abbreviated as CSC. The CSC were synthesized by a solution synthesis of polymer spheres followed by pyrolysis and self-deposition in the silica shell. As illustrated in Figure 1, the formation of hollow core−shell interlinked carbon spheres relied on the reconfiguration of solid nanospheres to the hollow core−shell structure aided by the hermetical silica shell. Briefly, solid polymer spheres (SPS) were synthesized by using resorcinol, formaldehyde, and 1,6-diaminohexane as the precursors.[39] If these polymer spheres were subject to a direct pyrolysis, solid carbon spheres were obtained (Figure 1, route 1). Instead, if the SPS were uniformly coated by a layer of silica enclosing a hermetical nanospace, during the pyrolysis process, polymer spheres were transformed into the carbon core accompanied by volume shrinkage, and the volatile carbonaceous species were deposited in the hermetical silica shell to form a layer of carbon/silica hybrid shell (Figure 1, route 2). Meanwhile, the newly formed carbon core has a higher surface energy, which exhibits a tendency to incidentally condense and sinter in the inner surface of the shell during temperature annealing, resulting in a core−shell interlinked structure. As a result, the CSC were obtained after etching the silica shells.

As seen in Figure 2a, the SPS are highly uniform with a diameter of *ca.* 370 nm. A higher magnification transmission electron microscopy (TEM) image (Figure 2b) clearly demonstrates its solid and dense nature. Subsequently, the SPS were coated with silica shells using cetyltrimethylammonium bromide (CTAB) as

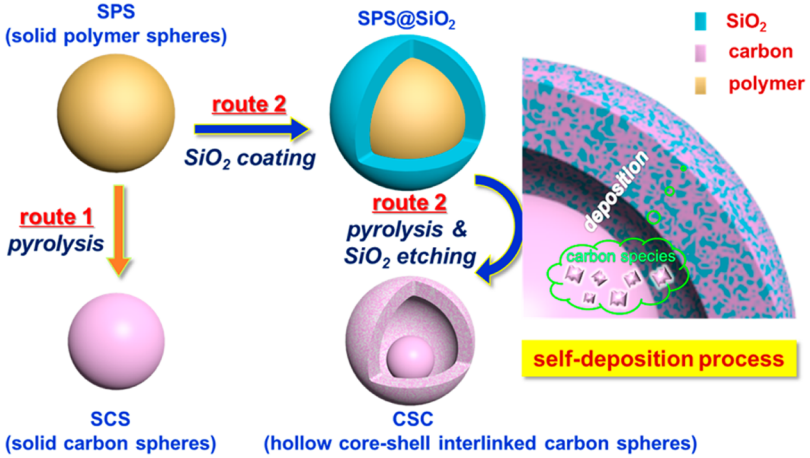

Figure 1. Schematic illustration of the synthesis of the hollow core−shell interlinked carbon spheres.

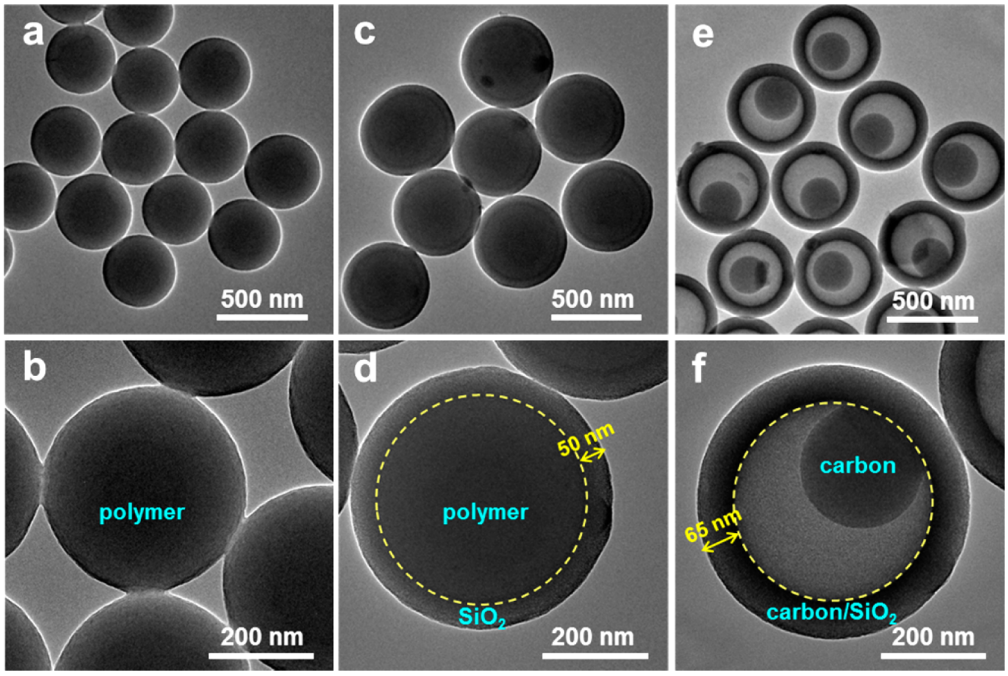

Figure 2. TEM images of (a,b) solid polymer nanospheres, (c,d) polymer/silica nanohybrids (SPS@SiO_2), and (e,f) carbon/silica hybrids (CSC@SiO_2).

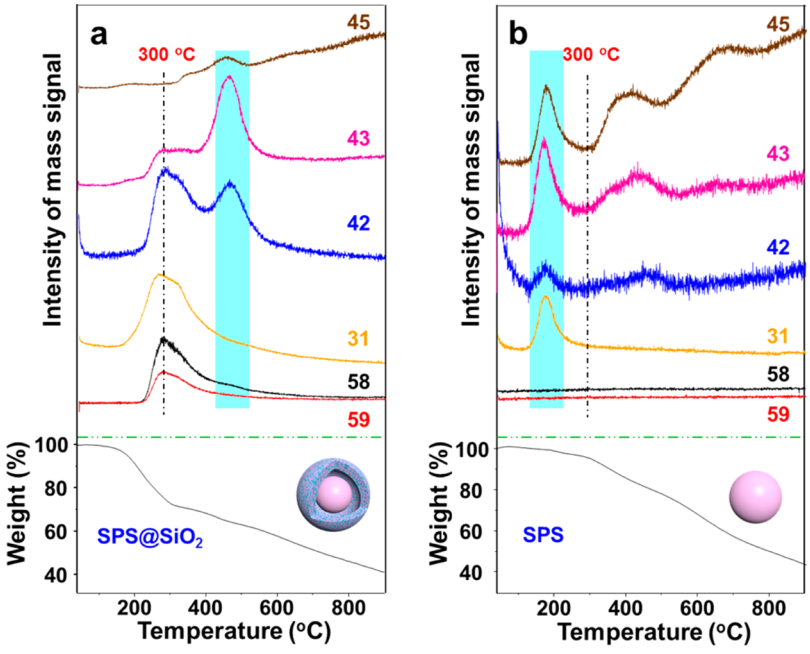

Figure 3. TG-MS measurements of the as-synthesized (a) SPS@SiO_2 and (b) SPS.

surfactant.[40,41] In Figure 2c,d, TEM images of the obtained polymer/silica nanohybrids (named SPS@SiO_2) show that each SPS is encapsulated by a silica shell with a thickness of *ca.* 50 nm. After pyrolysis, the inner polymer core was carbonized and the solid core–shell SPS@SiO_2 was converted to hollow core–shell carbon/silica hybrids with a void between the inner core (diameter = *ca.* 220 nm) and the outer shell (Figure 2e,f). The thickness of the outer shell is *ca.* 65 nm, which is 15 nm thicker than SPS@SiO_2 due to the carbon deposition during the pyrolysis process. For comparison, a control experiment, that is, direct pyrolysis of SPS, was carried out, and the result shows that solid carbon spheres (SCS) with a size of about 340 nm were obtained when there was no silica shell (see Supporting Information Figure S1).

To investigate the role of the silica shell during the pyrolysis process, the SPS and SPS@SiO_2 samples were characterized by TG-MS under Ar to monitor the onset of their thermal decomposition behavior (Figure 3). It is

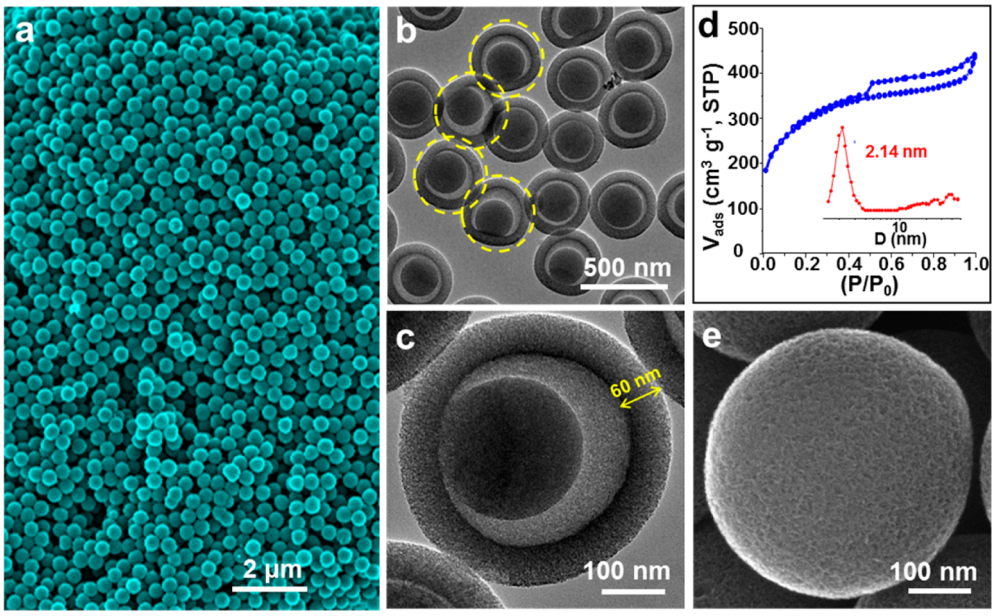

Figure 4. (a) SEM image, (b) TEM image, (c) high-resolution TEM image, (d) N_2 sorption isotherm and the pore size distribution (inset), and (e) high-resolution SEM image of CSC.

worth noting that the MS measurement is only used to qualitatively trace the volatile carbonaceous species, and to be clear, all the MS data given in Figure 3 were normalized. As seen from the TG curve of SPS@SiO_2 (Figure 3a), the weight loss between 150 and 300 °C corresponded to the CTAB decomposition.[41] Compared to SPS, it can be seen from the TG-MS curves that some volatile carbonaceous species (m/z = 31, 42, 43, and 45)[42] generated from SPS@SiO_2 are released at a temperature greater than 300 °C, where the ones generated from SPS release only at ~200 °C. It is because the volatile carbonaceous species generated from polymer decomposition are difficult to penetrate through the hermetical silica shells to arrive at the outer environment, as the silica shell is pressure-tight until CTAB decomposition. As a consequence, the majority of the volatile carbonaceous species deposit on the silica framework to form a carbon/silica hybrid shell. Meanwhile, the thermal constriction force tends to push the carbonaceous core that is stripped from the inner surface of the carbon/silica shell, giving rise to a hollow void. That is, a solid to hollow core−shell conversion occurred inside the hermetical silica shell during the pyrolysis process, which is similar to the Ostwald ripening process.[43]

After the SiO_2 shells were etched by NaOH solution, CSC were obtained. A large-area scanning electron microscopy (SEM) image (Figure 4a) proved that the carbon products have a uniform spherical morphology with a total size of approximately 410 nm, larger than the size (*ca.* 340 nm) of the SCS (Figure S1). Additional TEM images in Figure 4b,c show that the obtained CSC has a hollow void and, simultaneously, a carbonaceous core. By comparing the sizes of CSC and CSC@SiO_2, one can observe that their cores and shells remain almost identical in size, *ca.* 220 and 60 nm, respectively. These results, in turn, reveal that in the CSC@SiO_2 hybrids, the inner cores contain a carbon nanosphere and the shells comprise carbon and silica.

Nitrogen sorption measurement was further used to analyze the porosity of the obtained CSC. As seen in Figure 4d, the N_2 sorption isotherm reveals type-IV hysteresis, indicating a mesoporous characteristic, which suggests that the pores in the shell are accessible. The adsorption isotherm exhibits a slight step at a relative pressure (P/P_0) of 0.14−0.32, which corresponds to a pore size of 2.14 nm (inset in Figure 4d). The obtained CSC have a high Brunauer−Emmett−Teller (BET) surface area of 1038 m^2 g^{-1}, micropore surface area of 719 m^2 g^{-1}, and total pore volume of 0.69 cm^3 g^{-1}. The higher resolution SEM image (Figure 4e) of nanospheres clearly shows mesopores on the surface of the CSC, which also indicates the open pore structure of the carbon shell. Such mesopores account for the ready imbibition of sulfur into the carbon host.[32] Furthermore, the cracked sphere in the SEM image (Figure S2) shows the microporosity of the carbon core and void between the core and shell, consistent with our original design. However, unlike the CSC, the N_2 sorption isotherm of the SCS in Figure S3, which is derived from the direct pyrolysis of SPS, shows a type-I characteristic of a microporous material, and a relative low BET surface area of 626 m^2 g^{-1} is determined.

Besides having abundant pore structures and high surface area, another interesting feature of the CSC can be observed. That is, as seen in Figure 4b, in the structures marked with a yellow dashed box, the curvatures of spheres change to be relatively small, and the carbon cores seem to be anchored to the shells, which look like drupe fruit (Figure S4). For clarity, the TEM specimen of

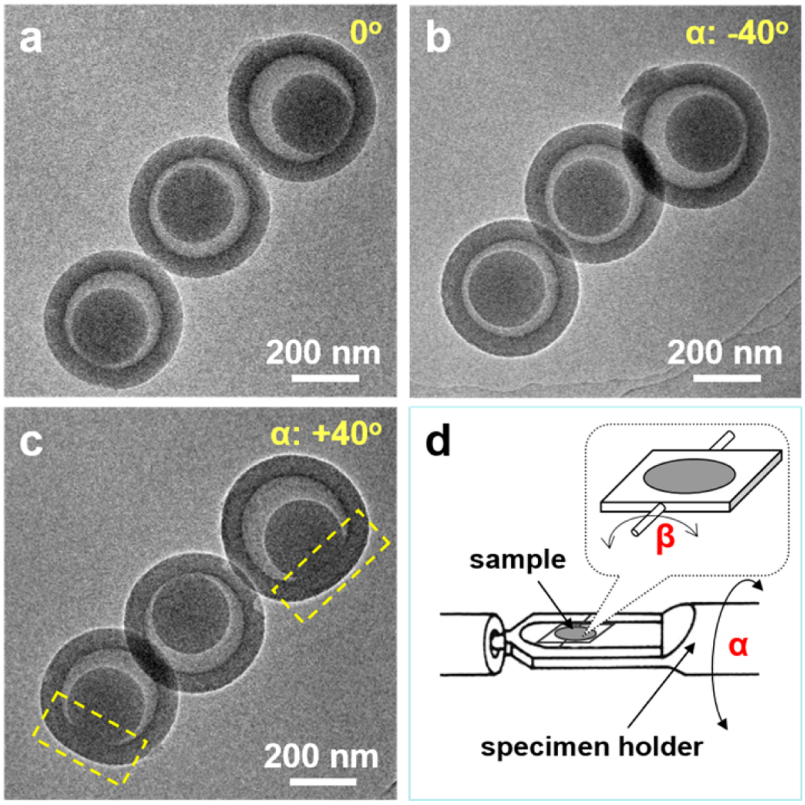

Figure 5. (a−c) TEM images of CSC with the sample holder tilted to −40, 0, and +40° by rotation around the axis of the holder. (d) Illustration of the TEM specimen holder tilting process.

CSC was carefully tilted by rotation around the axis of the holder to +40° and −40°, as illustrated in Figure 5. The TEM images with multiple views reveal that, though the cores look like they are "floating" inside, the core is indeed attached to the shell (Figures 5 and S5). To gain further insight on the formation mechanism of such a structure, the CSC@SiO_2 hybrid sample was also characterized by tilting the TEM specimen. As seen in Figure S6, the cores of the CSC@SiO_2 hybrids are also observed to be attached to the shell. These results further revealed that such "anchoring" of the carbon core to the inner surface of the shell took place during pyrolysis. During the SiO_2 etching process, a capillary pressure gradient is built in the interface of the core and shell, which is able to increase the contact surface area, resulting in the curvature reduction of the contact part of the carbon shell; as a consequence, the carbon with the most stable structure is spontaneously generated. This is the first observation of the one-step formation of a drupe-like nanocarbon in which the core is anchored on the interior surface of the shell.

The unique structure of CSC makes it a favorable substrate for accommodating and immobilizing the sulfur. A carbon−sulfur hybrid (CSC-S) was synthesized by a simple melt infiltration method. In the liquid state, sulfur can penetrate into the inner void through the outer porous shell. During the cooling process, the liquid sulfur solidifies and then is immobilized into the carbon matrix at room temperature. SEM and energy-dispersive X-ray (EDX) of CSC-S showed that no large sulfur particles were observed, and sulfur was homogeneously distributed in the nanocomposite by elemental mapping of carbon and sulfur (Figure S7). TEM and scanning transmission electron microscopy (STEM) images (Figures 6a,b and S8) showed that the CSC-S maintains a spherical morphology without distinguished hollow structure compared with CSC, where only a darker carbon core can be observed in a higher resolution TEM image (Figure S8). The above observations demonstrated that sulfur was well-encapsulated by the hollow core−shell structure. These results provided visible evidence that the core−shell interlinked structure effectively immobilized the sulfur inside the carbon matrix even under the strong electronic beam and ultrahigh vacuum of STEM. The sulfur content of 70 wt % (CSC-S-70) was confirmed by thermogravimetric analysis (TGA) (Figure 6c). Moreover, as seen from the TG curves, CSC-S-70 has a sulfur vaporizing temperature higher than that of the pure sulfur powder due to the enhanced interaction between the carbon matrix and sulfur.

The excellent penetration and confinement of the sulfur can be attributed to the capillarity interaction of liquid sulfur and the mesopores with the small size of ~2.14 nm[44] on the carbon shell; meanwhile, the micropore carbon cores inside the hollow structure possess high adsorption potential for sulfur.[6,21,45] Thus, this unique structure of the CSC-S composite not only

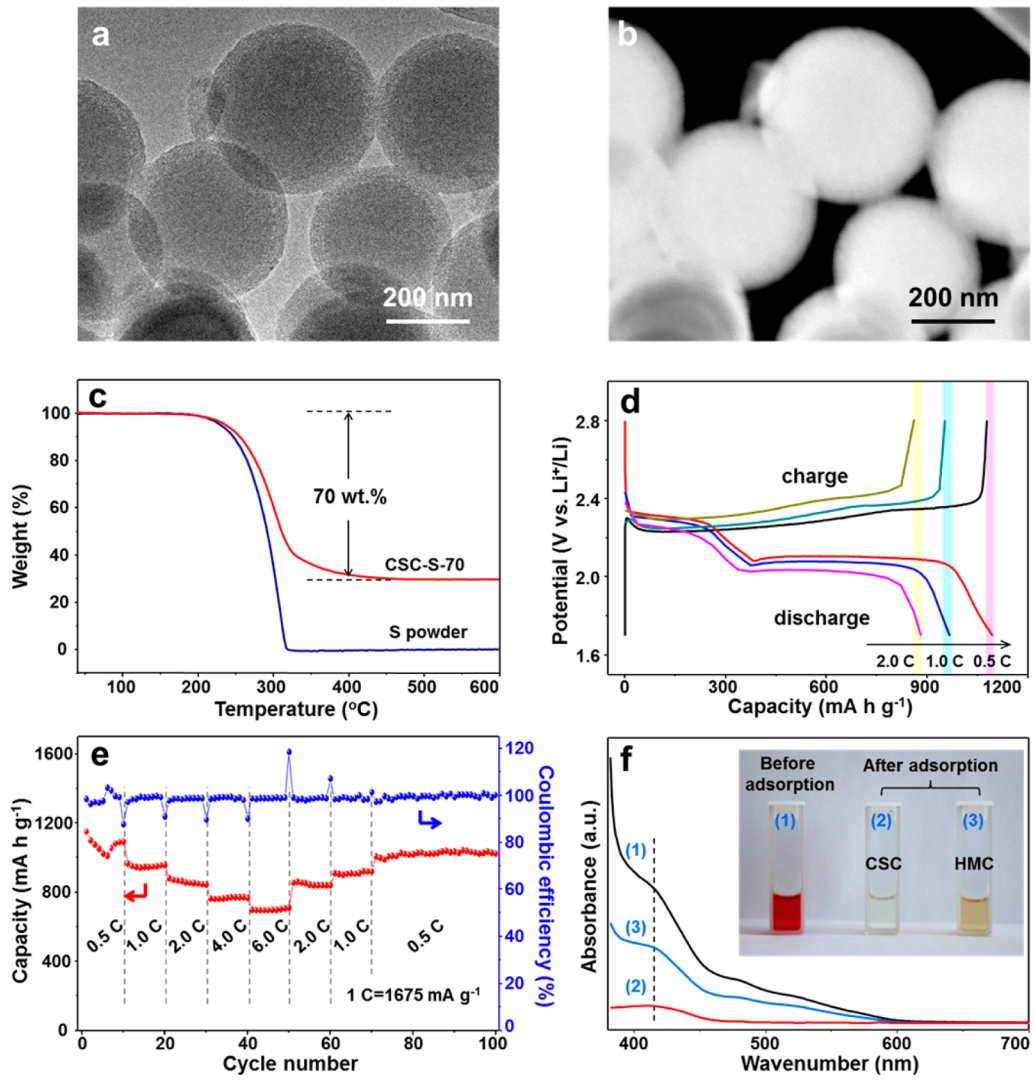

Figure 6. (a) TEM and (b) STEM images of CSC-S-70. (c) TGA curves of sulfur and CSC-S-70 in argon flow. (d) Galvanostatic discharge−charge profiles and (e) rate capabilities of CSC-S-70. (f) UV−vis spectra and associated color changes of a polysulfide solution before and after exposure to the CSC and HMC adsorbents.

enables the full utilization of the void but also renders the intimate contact of sulfur and carbon, which can facilitate the transportation of ions and help realize the full potential of the carbon−sulfur composite electrode.

The CSC-S-70 hybrid was then assembled into Li−S batteries to test its electrochemical performance. The capacity values are calculated on the basis of sulfur mass, unless otherwise stated. Typical discharge−charge voltage profiles of CSC-S between 1.7 and 2.8 V are presented in Figure 6d. The discharge curve at 0.5 C rate shows two plateaus around 2.3 and 2.1 V, which is the typical two-plateau behavior of sulfur cathodes.[46] At a 0.5 C rate, the CSC-S-70 cathode exhibits an initial discharge capacity of 1100 mAh g^{-1}. The corresponding capacity per electrode and area capacity were 577.5 mA h $g^{-1}_{electrode}$ (based on the total mass of CSC-S-70, conductive carbon and binder) and 1.1 mA h cm^{-2}_{sulfur}, respectively, which are comparable with recent reports on Li−S batteries.[28,47,48] After 10 cycles at 0.5 C, the CSC-S-70 electrode exhibits capacities of 950 and 860 mA h g^{-1} at 1.0 and 2.0 C, respectively, indicative of good rate performance and high stability. The rate capabilities of CSC-S-70 are shown in Figure 6e. The discharge capacity steadily changes as the current rates increase from 0.5 to 6.0 C. A capacity of *ca.* 700 mA h g^{-1} is obtained for CSC-S-70 at 6.0 C, and the cell recovers to almost the original 0.5 C capacity level, indicating the stability of such a unique nanocarbon cathode. The high capacity retention and Coulombic efficiency in CSC-S cathodes suggest that the microporous carbon core and mesoporous carbon shell play an important role in retarding polysulfide dissolution.

The performance of the CSC to trap polysulfide is shown in Figure 6f by comparing it with hollow mesoporous carbon spheres[49] without a microporous carbon core (HMC). The UV−vis spectra demonstrated that CSC can adsorb roughly twice as much polysulfide as the HMC. The color of the polysulfide solution also

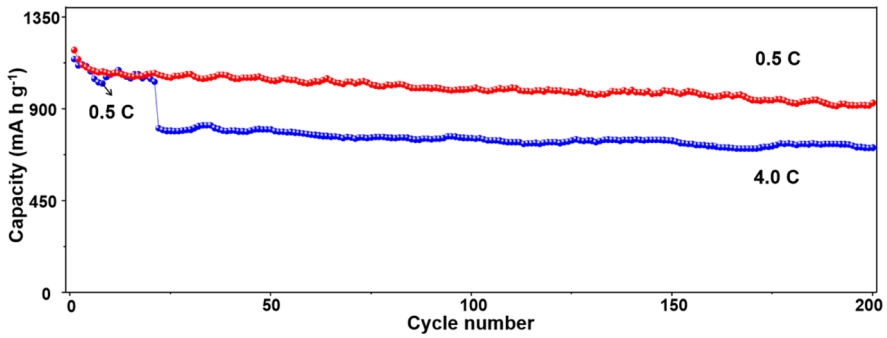

Figure 7. Cycling performance of CSC-S-70 at a current density of 0.5 and 4.0 C (1C = 1675 mA g^{-1}).

becomes much lighter after exposure to CSC (Figure 6f), further indicating the significant polysulfide adsorption ability of CSC nanostructures due to their small mesopore on the shell and the micropore carbon core. This result is in agreement with the reported literature that micropores can enhance the adsorption of polysulfides.[32] As discussed, the carbon host can not only immobilize the sulfur but also mitigate the diffusion of polysulfide.

Furthermore, different cycle behaviors evidently demonstrate the structural advantage of the hollow core−shell interlinked carbon spheres for sulfur immobilization. The CSC-S-70 electrode also possesses excellent cyclic stability (Figure 7). After continuous cycling for 200 cycles at a current density of 0.5 C, a reversible discharge capacity as high as 960 mA h g^{-1} is retained. When the current rate is switched from 0.5 to 4.0 C at the 20th cycle, the capacity remained at a value of *ca.* 730 mA h g^{-1} after another 180 cycles. To our knowledge, the electrochemical properties achieved in the CSC-S-70 are superior to that of the most reported porous carbons (Table S1), including hollow carbon spheres, carbon nanofibers, mesoporous carbon spheres, and so on.[34,50−52] Importantly, CSC-S electrodes also show significant capacity with increasing sulfur content in the cathodes. For instance, by increasing the sulfur ratio to 85 wt % (TG result in Figure S9) in the carbon−sulfur hybrid (CSC-S-85), the initial capacity of the sample still remained *ca.* 890 mA h g^{-1} at 0.4 C. In addition, the discharge capacities still remain with 720 and 590 mA h g^{-1} at 0.4 and 3.2 C after 200 cycles, respectively (Figure S10).

Such good electrochemical performance of the CSC-S hybrid may be attributed to the easy electronic/ionic transport. Compared to the solid carbon spheres or hollow mesoporous spheres, the hollow core−shell carbon spheres concurrently have a mesoporous shell, a hollow void, and a microporous core, which greatly shortens the diffusion distance of Li ions and enhances the electrical conductivity. In addition, as depicted in Figure S11, after 200 cycles, the hollow core−shell structure of the carbon host still remained well-defined, indicating that CSC allow sulfur to alleviate its mechanical strain without forming cracks and pulverization upon lithiation/delithiation, which accounts for the outstanding cycle stability of CSC-S cathodes. One can envisage that the performance of CSC-S with high sulfur loading can be further promoted by incorporating heteroatoms (*e.g.*, nitrogen doping)[18,53] or metal oxide[54,55] into the structure for chemical adsorption of polysulfides. Thus, the CSC-S battery with high areal sulfur loading will be promising in practical applications requiring high energy density.[56]

CONCLUSIONS

A new type of hollow core−shell carbon sphere has been synthesized. This new carbon nanoarchitecture concurrently has three interconnected parts: a mesoporous shell, a hollow void, and a microporous core anchored to the shell, which is very useful to confine sulfur-active materials. A significant improvement not only in the active material utilization but also in capacity retention can be observed. The microporous carbon core anchored on the shell decreases the internal charge transfer resistance and localizes the soluble polysulfides, facilitating a stable cycle performance. The carbon−sulfur cathodes show a high utilization of sulfur with a desirable loading of 70 wt % and exhibit excellent cycling stability, that is, 960 mA h g^{-1} after 200 cycles at a current density of 0.5 C. Furthermore, such a carbon−sulfur composite electrode still has excellent cycle stability and rate capability with increasing sulfur content to 85 wt %. We believe our results will provide an impetus to exploit new structures and candidates for high-performance Li ion batteries.

METHODS

Materials. Resorcinol (99.5%), formaldehyde (37 wt %), 1,6-diaminohexane (DAH, 99.0%), CTAB (99%), and tetraethyl orthosilicate (TEOS) were supplied by Sinopharm Chemical Reagent Co., Ltd. All chemicals were used as received without any further purification.

Synthesis of Solid Polymer Nanosphere and Solid Carbon Nanosphere. SPS were prepared according to a modified method reported by our group.[39] Typically, resorcinol (2 mmol) was first dissolved in

deionized water, and then formaldehyde (37 wt %) (4 mmol) was added to form a clear solution at the initial reaction temperature of 28 °C. After the addition of DAH (0.5 mmol), the clear solution became a white colloid within a minute and stirring was continued for 30 min. Fifty microliters of ammonia was then added to this solution. The resultant solution was further heated to 80 °C for another 4 h. Then, the polymer products were purified three times with water by centrifugation at a speed of 8000 rpm. SCS were obtained by pyrolyzing SPS at 900 °C for 2 h under argon flow.

Synthesis of Hollow Core−Shell Carbon. To produce the silica coating, SPS were stirred with ethanol and deionized water mixed with an aqueous ammonia solution. Subsequently, a CTAB solution was added to the latex while stirring for 30 min. This solution was vigorously stirred for a further 30 min before TEOS was added, and the stirring continued for 16 h at room temperature. The SPS@SiO_2 was washed, dried, and then pyrolyzed at 900 °C for 2 h under an argon flow to obtain CSC@SiO_2. CSC were obtained using 1.875 M NaOH alcohol−water (the volume ratio of alcohol to water was 1:3) solution to treat the CSC@SiO_2 at 50 °C for 24 h. EDX analysis showed no silica signal, indicating that the silica had been etched off.

Synthesis of Carbon−Sulfur Hybrids. The as-prepared carbon products and sulfur were ground together, heated to 155 °C in a sealed vacuum tube, and kept there for 20 h to facilitate sulfur diffusion into the carbon host. Then, the hybrid was washed using alcohol−carbon disulfide (the volume ratio of alcohol to carbon disulfide was 9:1) solution to clean the sulfur deposited on its outside surface.

Adsorption of Lithium Polysulfide. Lithium polysulfide (Li_2S_6) was synthesized according to the literature. Typically, the stoichiometric amounts of sulfur (S) and lithium sulfide (Li_2S) with a molar ratio of 5:1 were dissolved in tetrahydrofuran by being magnetically stirred at room temperature under an argon atmosphere, yielding a burgundy solution.

The adsorption ability of the hollow CSC and HMC on lithium polysulfide was investigated by UV−vis spectroscopy. Typically, 100 mg of each carbon host was placed in 10 mL of Li_2S_6 solution (10 mM), and the mixture was stirred for 15 min. The concentration of residual lithium polysulfide in the solution was determined by UV−vis adsorption at 415 nm. The adsorption capacity was calculated by the following equation:

$$\text{adsorption capacity (g/g)} = [(C_0 - C_r)] \times V \times M]/m$$

where C_0 is the molar concentration of Li_2S_6 solution before adsorption; C_r is the molar concentration of Li_2S_6 solution after adsorption; V is the volume of the Li_2S_6 solution used in the adsorption test; M is the molar mass of Li_2S_6; and m is the mass of adsorbent.

The adsorption capacities of Li_2S_6 on CSC and HMC are about 0.15 and 0.10 g/g, respectively.

Electrochemical Characterization. Electrochemical experiments were performed using CR2025 coin-type test cells assembled at room temperature in an argon-filled glovebox with lithium metal as the counter electrode. The cathode for the Li−S batteries was prepared by mixing 75 wt % of the carbon−sulfur hybrid, 15 wt % conductive carbon, and 10 wt % LA133 in water to form a slurry. Subsequently, the slurry was pasted onto a carbon-coated aluminum foil, and a Celgard 2400 membrane was used as the separator to isolate electrons. The loading capability of sulfur in the cathodes was about 1.0 mg cm^{-2}. The electrolyte was 1 M bis(trifluoromethane)sulfonimide lithium salt that was dissolved in a mixture of 1,3-dioxolane and dimethoxymethane (1:1 by volume) with 2 wt % $LiNO_3$ as an additive. Twenty microliters of electrolyte was used to construct each Li−S cell. The density, ρ, of the electrolyte is ~1.1 g cm^{-3}. So the mass of the electrolyte is 22 mg. As a result, the E/S ratio is *ca.* 22, which is lower than that in most reported works.[48,57] The discharge−charge measurements were conducted in the voltage range of 1.7−2.8 V using a Land CT2001A battery test system.

Characterization. SEM and EDX were carried out with a FEI Nova NanoSEM 450 instrument. TEM analyses were carried out with a FEI Tecnai $G^2$20S-Twin instrument operating at 200 kV. STEM was performed with a FEI Tecnai F30 electron microscope. The samples for TEM and STEM analyses were prepared by dropping an ethanol droplet of the products on carbon-coated copper grids and drying at room temperature. The nitrogen sorption isotherm was measured with a Micromeritics ASAP 2020 adsorption analyzer at 77 K. Before the measurements, all samples were degassed at 200 °C for 6 h. The specific surface areas (S_{BET}) were calculated from the adsorption data in the relative pressure range of 0.05−0.3 using the BET method. Pore size distributions were determined from the adsorption branch of the isotherm using density functional theory. The total pore volume (V_{total}) was estimated from the amount adsorbed at a relative pressure of 0.99. TG-MS was conducted on a STA 449 F3 (NETZSCH) thermogravimetric analyzer coupled with an OmniStar GSD 320 mass spectrometer, under an argon flow with a heating rate of 10 °C min^{-1}. The adsorption performance of lithium polysulfide was measured using a UV−vis spectrophotometer.

Conflict of Interest: The authors declare no competing financial interest.

Supporting Information Available: Additional figures, and tables. The Supporting Information is available free of charge on the ACS Publications website at DOI: 10.1021/acsnano.5b03488.

Acknowledgment. This project was financially supported by National Science Fund for National Natural Science Foundation of China (Nos. 21225312 and 21473021).

REFERENCES AND NOTES

1. Ji, X.; Nazar, L. F. Advances in Li-S Batteries. *J. Mater. Chem.* **2010**, *20*, 9821–9826.
2. Manthiram, A.; Fu, Y.; Su, Y.-S. Challenges and Prospects of Lithium-Sulfur Batteries. *Acc. Chem. Res.* **2013**, *46*, 1125–1134.
3. Evers, S.; Nazar, L. F. New Approaches for High Energy Density Lithium−Sulfur Battery Cathodes. *Acc. Chem. Res.* **2013**, *46*, 1135–1143.
4. Bruce, P. G.; Freunberger, S. A.; Hardwick, L. J.; Tarascon, J. M. Li-O_2 and Li-S Batteries with High Energy Storage. *Nat. Mater.* **2012**, *11*, 19–29.
5. Guo, J.; Xu, Y.; Wang, C. Sulfur-Impregnated Disordered Carbon Nanotubes Cathode for Lithium−Sulfur Batteries. *Nano Lett.* **2011**, *11*, 4288–4294.
6. Chen, H.; Wang, C.; Dong, W.; Lu, W.; Du, Z.; Chen, L. Monodispersed Sulfur Nanoparticles for Lithium-Sulfur Batteries with Theoretical Performance. *Nano Lett.* **2015**, *15*, 798–802.
7. Xin, S.; Gu, L.; Zhao, N.-H.; Yin, Y.-X.; Zhou, L.-J.; Guo, Y.-G.; Wan, L.-J. Smaller Sulfur Molecules Promise Better Lithium-Sulfur Batteries. *J. Am. Chem. Soc.* **2012**, *134*, 18510–18513.
8. Suo, L.; Hu, Y.-S.; Li, H.; Armand, M.; Chen, L. A New Class of Solvent-in-Salt Electrolyte for High-Energy Rechargeable Metallic Lithium Batteries. *Nat. Commun.* **2013**, *4*, 1481–1489.
9. Zhou, G.; Pei, S.; Li, L.; Wang, D.-W.; Wang, S.; Huang, K.; Yin, L.-C.; Li, F.; Cheng, H.-M. A Graphene-Pure-Sulfur Sandwich Structure for Ultrafast, Long-Life Lithium-Sulfur Batteries. *Adv. Mater.* **2014**, *26*, 625–631.
10. Ai, X.-P.; Cao, Y.-L.; Yang, H.-X. Simple Analysis and Possible Solutions of the Unusual Interfacial Reactions in Li-S Batteries. *J. Electrochem.* **2012**, *18*, 224–228.
11. Zhou, L.; Lin, X.; Huang, T.; Yu, A. Nitrogen-Doped Porous Carbon Nanofiber Webs/Sulfur Composites as Cathode Materials for Lithium-Sulfur Batteries. *Electrochim. Acta* **2014**, *116*, 210–216.
12. Wang, H.; Yang, Y.; Liang, Y.; Robinson, J. T.; Li, Y.; Jackson, A.; Cui, Y.; Dai, H. Graphene-Wrapped Sulfur Particles as a Rechargeable Lithium−Sulfur Battery Cathode Material with High Capacity and Cycling Stability. *Nano Lett.* **2011**, *11*, 2644–2647.
13. Wang, D.-W.; Zeng, Q.; Zhou, G.; Yin, L.; Li, F.; Cheng, H.-M.; Gentle, I. R.; Lu, G. Q. Carbon-Sulfur Composites for Li-S Batteries: Status and Prospects. *J. Mater. Chem. A* **2013**, *1*, 9382–9394.

14. Wang, J. L.; Yang, J.; Xie, J. Y.; Xu, N. X.; Li, Y. Sulfur-Carbon Nano-Composite as Cathode for Rechargeable Lithium Battery Based on Gel Electrolyte. *Electrochem. Commun.* **2002**, *4*, 499–502.
15. Wang, J.; Liu, L.; Ling, Z.; Yang, J.; Wan, C.; Jiang, C. Polymer Lithium Cells with Sulfur Composites as Cathode Materials. *Electrochim. Acta* **2003**, *48*, 1861–1867.
16. Han, F.; Li, W.-C.; Li, D.; Lu, A.-H. *In Situ* Electrochemical Generation of Mesostructured Cu_2S/C Composite for Enhanced Lithium Storage: Mechanism and Material Properties. *ChemElectroChem* **2014**, *1*, 733–740.
17. Li, D.; Han, F.; Wang, S.; Cheng, F.; Sun, Q.; Li, W.-C. High Sulfur Loading Cathodes Fabricated Using Peapodlike, Large Pore Volume Mesoporous Carbon for Lithium-Sulfur Battery. *ACS Appl. Mater. Interfaces* **2013**, *5*, 2208–2213.
18. Song, J.; Gordin, M. L.; Xu, T.; Chen, S.; Yu, Z.; Sohn, H.; Lu, J.; Ren, Y.; Duan, Y.; Wang, D. Strong Lithium Polysulfide Chemisorption on Electroactive Sites of Nitrogen-Doped Carbon Composites for High-Performance Lithium-Sulfur Battery Cathodes. *Angew. Chem., Int. Ed.* **2015**, *54*, 4325–4329.
19. Zhang, X.-Q.; Sun, Q.; Dong, W.; Li, D.; Lu, A.-H.; Mu, J.-Q.; Li, W.-C. Synthesis of Superior Carbon Nanofibers with Large Aspect Ratio and Tunable Porosity for Electrochemical Energy Storage. *J. Mater. Chem. A* **2013**, *1*, 9449–9455.
20. Ji, X.; Lee, K. T.; Nazar, L. F. A Highly Ordered Nanostructured Carbon-Sulphur Cathode for Lithium-Sulphur Batteries. *Nat. Mater.* **2009**, *8*, 500–506.
21. Li, Z.; Jiang, Y.; Yuan, L.; Yi, Z.; Wu, C.; Liu, Y.; Strasser, P.; Huang, Y. A Highly Ordered Meso@Microporous Carbon-Supported Sulfur@Smaller Sulfur Core-Shell Structured Cathode for Li-S Batteries. *ACS Nano* **2014**, *8*, 9295–9303.
22. Schneider, A.; Weidmann, C.; Suchomski, C.; Sommer, H.; Janek, J.; Brezesinski, T. Ionic Liquid-Derived Nitrogen-Enriched Carbon/Sulfur Composite Cathodes with Hierarchical Microstructure—A Step toward Durable High-Energy and High-Performance Lithium-Sulfur Batteries. *Chem. Mater.* **2015**, *27*, 1674–1683.
23. Chen, L.; Shaw, L. L. Recent Advances in Lithium-Sulfur Batteries. *J. Power Sources* **2014**, *267*, 770–783.
24. Manthiram, A.; Fu, Y.; Chung, S.-H.; Zu, C.; Su, Y.-S. Rechargeable Lithium-Sulfur Batteries. *Chem. Rev.* **2014**, *114*, 11751–11787.
25. Brun, N.; Sakaushi, K.; Yu, L.; Giebeler, L.; Eckert, J.; Titirici, M. M. Hydrothermal Carbon-Based Nanostructured Hollow Spheres as Electrode Materials for High-Power Lithium-Sulfur Batteries. *Phys. Chem. Chem. Phys.* **2013**, *15*, 6080–6087.
26. Jayaprakash, N.; Shen, J.; Moganty, S. S.; Corona, A.; Archer, L. A. Porous Hollow Carbon@Sulfur Composites for High-Power Lithium-Sulfur Batteries. *Angew. Chem., Int. Ed.* **2011**, *50*, 5904–5908.
27. He, G.; Evers, S.; Liang, X.; Cuisinier, M.; Garsuch, A.; Nazar, L. F. Tailoring Porosity in Carbon Nanospheres for Lithium-Sulfur Battery Cathodes. *ACS Nano* **2013**, *7*, 10920–10930.
28. Peng, H.-J.; Liang, J.; Zhu, L.; Huang, J.-Q.; Cheng, X.-B.; Guo, X.; Ding, W.; Zhu, W.; Zhang, Q. Catalytic Self-Limited Assembly at Hard Templates: A Mesoscale Approach to Graphene Nanoshells for Lithium-Sulfur Batteries. *ACS Nano* **2014**, *8*, 11280–11289.
29. Li, Z.; Yuan, L.; Yi, Z.; Sun, Y.; Liu, Y.; Jiang, Y.; Shen, Y.; Xin, Y.; Zhang, Z.; Huang, Y. Insight into the Electrode Mechanism in Lithium-Sulfur Batteries with Ordered Microporous Carbon Confined Sulfur as the Cathode. *Adv. Energy Mater.* **2014**, *4*, 1301473.
30. Wang, D.-W.; Zhou, G.; Li, F.; Wu, K.-H.; Lu, G. Q.; Cheng, H.-M.; Gentle, I. R. A Microporous-Mesoporous Carbon with Graphitic Structure for a High-Rate Stable Sulfur Cathode in Carbonate Solvent-Based Li-S Batteries. *Phys. Chem. Chem. Phys.* **2012**, *14*, 8703–8710.
31. Zhang, B.; Qin, X.; Li, G. R.; Gao, X. P. Enhancement of Long Stability of Sulfur Cathode by Encapsulating Sulfur into Micropores of Carbon Spheres. *Energy Environ. Sci.* **2010**, *3*, 1531–1537.
32. Yang, C.-P.; Yin, Y.-X.; Guo, Y.-G.; Wan, L.-J. Electrochemical (De) Lithiation of 1D Sulfur Chains in Li-S Batteries: A Model System Study. *J. Am. Chem. Soc.* **2015**, *137*, 2215–2218.
33. Schuster, J.; He, G.; Mandlmeier, B.; Yim, T.; Lee, K. T.; Bein, T.; Nazar, L. F. Spherical Ordered Mesoporous Carbon Nanoparticles with High Porosity for Lithium-Sulfur Batteries. *Angew. Chem., Int. Ed.* **2012**, *51*, 3591–3595.
34. He, G.; Ji, X.; Nazar, L. F. High "C" Rate Li-S Cathodes: Sulfur Imbibed Bimodal Porous Carbons. *Energy Environ. Sci.* **2011**, *4*, 2878–2883.
35. Yang, Y.; Yu, G.; Cha, J. J.; Wu, H.; Vosgueritchian, M.; Yao, Y.; Bao, Z.; Cui, Y. Improving the Performance of Lithium–Sulfur Batteries by Conductive Polymer Coating. *ACS Nano* **2011**, *5*, 9187–9193.
36. Li, X.; Cao, Y.; Qi, W.; Saraf, L. V.; Xiao, J.; Nie, Z.; Mietek, J.; Zhang, J.-G.; Schwenzer, B.; Liu, J. Optimization of Mesoporous Carbon Structures for Lithium-Sulfur Battery Applications. *J. Mater. Chem.* **2011**, *21*, 16603–16610.
37. Liang, C. D.; Dudney, N. J.; Howe, J. Y. Hierarchically Structured Sulfur/Carbon Nanocomposite Material for High-Energy Lithium Battery. *Chem. Mater.* **2009**, *21*, 4724–4730.
38. Zheng, G.; Yang, Y.; Cha, J. J.; Hong, S. S.; Cui, Y. Hollow Carbon Nanofiber-Encapsulated Sulfur Cathodes for High Specific Capacity Rechargeable Lithium Batteries. *Nano Lett.* **2011**, *11*, 4462–4467.
39. Wang, S.; Li, W.-C.; Hao, G.-P.; Hao, Y.; Sun, Q.; Zhang, X.-Q.; Lu, A.-H. Temperature-Programmed Precise Control over the Sizes of Carbon Nanospheres Based on Benzoxazine Chemistry. *J. Am. Chem. Soc.* **2011**, *133*, 15304–15307.
40. Lu, A.-H.; Sun, T.; Li, W.-C.; Sun, Q.; Liu, D.-H.; Guo, Y. Synthesis of Discrete and Dispersible Hollow Carbon Nanospheres with High Uniformity by Using Confined Nanospace Pyrolysis. *Angew. Chem., Int. Ed.* **2011**, *50*, 11765–11768.
41. Sun, Q.; Li, W.-C.; Lu, A.-H. Insight into Structure-Dependent Self-Activation Mechanism in a Confined Nanospace of Core-Shell Nanocomposites. *Small* **2013**, *9*, 2086–2090.
42. Kleitz, F.; Schmidt, W.; Schüth, F. Calcination Behavior of Different Surfactant-Templated Mesostructured Silica Materials. *Microporous Mesoporous Mater.* **2003**, *65*, 1–29.
43. Zeng, H. C. Ostwald Ripening: A Synthetic Approach for Hollow Nanomaterials. *Curr. Nanosci.* **2007**, *3*, 177–181.
44. Zhou, W.; Wang, C.; Zhang, Q.; Abruña, H. D.; He, Y.; Wang, J.; Mao, S. X.; Xiao, X. Tailoring Pore Size of Nitrogen-Doped Hollow Carbon Nanospheres for Confining Sulfur in Lithium-Sulfur Batteries. *Adv. Energy Mater.* **2015**, 1401752.
45. Jung, D. S.; Hwang, T. H.; Lee, J. H.; Koo, H. Y.; Shakoor, R. A.; Kahraman, R.; Jo, Y. N.; Park, M.-S.; Choi, J. W. Hierarchical Porous Carbon by Ultrasonic Spray Pyrolysis Yields Stable Cycling in Lithium-Sulfur Battery. *Nano Lett.* **2014**, *14*, 4418–4425.
46. Su, Y.-S.; Fu, Y.; Cochell, T.; Manthiram, A. A Strategic Approach to Recharging Lithium-Sulphur Batteries for Long Cycle Life. *Nat. Commun.* **2013**, *4*, 2985–2992.
47. Yang, X.; Zhang, L.; Zhang, F.; Huang, Y.; Chen, Y. Sulfur-Infiltrated Graphene-Based Layered Porous Carbon Cathodes for High-Performance Lithium Sulfur Batteries. *ACS Nano* **2014**, *8*, 5208–5219.
48. Zhao, M.-Q.; Zhang, Q.; Huang, J.-Q.; Tian, G.-L.; Nie, J.-Q.; Peng, H.-J.; Wei, F. Unstacked Double-Layer Templated Graphene for High-Rate Lithium-Sulphur Batteries. *Nat. Commun.* **2014**, *5*, 3410.
49. Yoon, S. B.; Sohn, K.; Kim, J. Y.; Shin, C.-H.; Yu, J.-S.; Hyeon, T. Fabrication of Carbon Capsules with Hollow Macroporous Core/Mesoporous Shell Structures. *Adv. Mater.* **2002**, *14*, 19–21.
50. Zhang, C.; Wu, H. B.; Yuan, C.; Guo, Z.; Lou, X. W. Confining Sulfur in Double-Shelled Hollow Carbon Spheres for Lithium-Sulfur Batteries. *Angew. Chem., Int. Ed.* **2012**, *51*, 9592–9595.
51. Yao, H.; Zheng, G.; Li, W.; McDowell, M. T.; Seh, Z.; Liu, N.; Lu, Z.; Cui, Y. Crab Shells as Sustainable Templates from

Nature for Nanostructured Battery Electrodes. *Nano Lett.* **2013**, *13*, 3385–3390.
52. Zheng, G.; Zhang, Q.; Cha, J. J.; Yang, Y.; Li, W.; Seh, Z. W.; Cui, Y. Amphiphilic Surface Modification of Hollow Carbon Nanofibers for Improved Cycle Life of Lithium Sulfur Batteries. *Nano Lett.* **2013**, *13*, 1265–1270.
53. Peng, H.-J.; Hou, T.-Z.; Zhang, Q.; Huang, J.-Q.; Cheng, X.-B.; Guo, M.-Q.; Yuan, Z.; He, L.-Y.; Wei, F. Strongly Coupled Interfaces Between a Heterogeneous Carbon Host and a Sulfur-Containing Guest for Highly Stable Lithium-Sulfur Batteries: Mechanistic Insight into Capacity Degradation. *Adv. Mater. Interfaces* **2014**, *1*, 1400227.
54. Hart, C. J.; Cuisinier, M.; Liang, X.; Kundu, D.; Garsuch, A.; Nazar, L. F. Rational Design of Sulphur Host Materials for Li-S Batteries: Correlating Lithium Polysulphide Adsorptivity and Self-Discharge Capacity Loss. *Chem. Commun.* **2015**, *51*, 2308–2311.
55. Liang, X.; Hart, C.; Pang, Q.; Garsuch, A.; Weiss, T.; Nazar, L. F. A Highly Efficient Polysulfide Mediator for Lithium–Sulfur Batteries. *Nat. Commun.* **2015**, *6*, 5682.
56. Zhu, L.; Peng, H. J.; Liang, J.; Huang, J. Q.; Chen, C. M.; Guo, X.; Zhu, W.; Li, P.; Zhang, Q. Interconnected Carbon Nanotube/Graphene Nanosphere Scaffolds as Free-Standing Paper Electrode for High-Rate and Ultra-Stable Lithium-Sulfur Batteries. *Nano Energy* **2015**, *11*, 746–755.
57. Tang, C.; Zhang, Q.; Zhao, M.-Q.; Huang, J.-Q.; Cheng, X.-B.; Tian, G.-L.; Peng, H.-J.; Wei, F. Nitrogen-Doped Aligned Carbon Nanotube/Graphene Sandwiches: Facile Catalytic Growth on Bifunctional Natural Catalysts and Their Applications as Scaffolds for High-Rate Lithium-Sulfur Batteries. *Adv. Mater.* **2014**, *26*, 6100–6111.